Research Article GU J Sci, Part A, 10(4): 417-441 (2023) 10.54287/gujsa.1357216

Gazi University
Journal of Science
PART A: ENGINEERING AND INNOVATION
http://dergipark.org.tr/gujsa

# FOPID Controller Design for a Buck Converter System Using a Novel Hybrid Cooperation Search Algorithm with Pattern Search for Parameter Tuning

Cihan ERSALI [1*] Baran HEKİMOĞLU [1]

[1] Department of Electrical and Electronics Engineering, Batman University, Batman, Türkiye

**Keywords**

FOPID Controller
Buck Converter
Cooperation Search Algorithm
Pattern Search
Opposition-Based Learning

**Abstract**

This research introduces a novel metaheuristic algorithm, OCSAPS, representing an upgraded cooperation search algorithm (CSA) version. OCSAPS incorporates opposition-based learning (OBL) and pattern search (PS) algorithms. The proposed algorithm's application aims to develop a fractional order proportional-integral-derivative (FOPID) controller tailored for a buck converter system. The efficacy of the proposed algorithm is assessed by statistical boxplot and convergence response analyses. Furthermore, the performance of the OCSAPS-based FOPID-controlled buck converter system is benchmarked against CSA, Harris hawk optimization (HHO), and genetic algorithm (GA). This comparative analysis encompasses transient and frequency responses, performance indices, and robustness analysis. The outcomes of this comparison highlight the distinctive advantages of the proposed approach-based system. Moreover, the proposed approach's performance was compared with six other approaches used to control buck converter systems similarly regarding both time and frequency domain responses. Overall, the findings underscore the efficacy of the OCSAPS algorithm as a robust solution for designing FOPID controllers in buck converter systems.

**Cite**

Ersali, C., & Hekimoglu, B. (2023). FOPID Controller Design for a Buck Converter System Using a Novel Hybrid Cooperation Search Algorithm with Pattern Search for Parameter Tuning. *GU J Sci, Part A, 10*(4), 417-441. doi:10.54287/gujsa.1357216

**Author ID (ORCID Number)**

0000-0001-8368-1195 Cihan ERSALI
0000-0002-1839-025X Baran HEKİMOĞLU

**Article Process**

**Submission Date** 08.09.2023
**Revision Date** 10.10.2023
**Accepted Date** 25.10.2023
**Published Date** 11.12.2023

## 1. INTRODUCTION

Over the past decade, there has been a surge in the popularity of battery-powered iterations of corded electronic devices like household appliances and consumer electronics. The convenience and portability drive this trend that these battery-powered versions offer. These devices rely on power electronics converters to ensure optimal DC-DC voltage and power utilization within their circuits. The buck converter has emerged as a favored choice for regulating and fine-tuning output voltage in these devices (Zhang & Qiu, 2014). Its widespread adoption is attributed to its simplicity, low cost, uncomplicated structure, and exceptional dynamic performance, making it versatile for various applications, including power conversion and motor drives (Lee et al., 1997). Designing a standout controller for the DC-DC buck converter is critical for establishing stable, efficient, and reliable systems. However, the inherent nonlinear characteristics of buck converters pose challenges in controller design (Wang et al., 2017). Researchers have responded to these challenges by exploring diverse controller types to achieve the desired system qualities (Al-Majidi et al., 2019).

There have been extensive studies utilizing different types of optimization approaches for DC-DC buck converters. In Izci et al. (2002a) and Izci and Ekinci (2022), state-of-the-art metaheuristic algorithms have been used to optimize FOPID controllers for DC-DC buck converters, which are some of the best-performing systems in the field. In Izci et al. (2002a) a hybrid version of the Levy flight distribution (LFD) algorithm is utilized to optimize a FOPID controller for the buck converter. The algorithm they proposed resulted in a

*Corresponding Author, e-mail: cihan.ersali@batman.edu.tr

12.9% better transient response and 14.8% better frequency response compared to the original LFD. Izci and Ekinci (2022) proposed an improved version of the hunger games search (HGS) algorithm to optimally control a FOPID controller for a DC-DC buck converter. They obtained a 21.8% faster rise time and 27.9% more bandwidth than the original HGS algorithm.

Similarly, in Sangeetha et al. (2023), a FOPID controller has been optimized for a DC-DC buck converter using a hybrid of Golden Jackal Optimization (GJO) and Capuchin Search Algorithm (CapSA), which they proposed in their study. They managed to improve the efficiency by 12.9% compared to the second-best method in their study, which is the genetic algorithm (GA). They also reduced the cost by 18.9% compared to particle swarm optimization (PSO).

In Warrier & Shah (2021), a cohort intelligence (CI) optimization has been used to optimize a FOPID controller for a DC-DC buck converter. They achieved 61.6% less overshoot and 24.7% less computation time compared to second best approaches reported in their study.

Effective controllers are expected to exhibit stability, robustness, swift transient response, accurate tracking, and precise frequency response. PID controllers are the most popular due to their straightforward structure, adaptability, and wide-scale industrial application (Hsieh & Chou, 2007). Despite the advantages of PID controllers, their parameter-tuning process is often laborious, relying on trial and error. Moreover, scenarios involving nonlinear effects, load fluctuations, disturbances, and parameter changes challenge the efficacy of PID controllers. This has spurred the need for more advanced control strategies (Monje et al., 2008).

In recent decades, fractional calculus and its application, particularly fractional control, have captivated the interest of researchers (Shah & Agashe, 2016; Ortiz-Quisbert et al., 2018; Chevalier et al., 2019; Micev et al., 2020; Dolai et al., 2022). FOPID controllers offer increased flexibility by incorporating fractional integral ($\lambda$) and derivative ($\mu$) terms, making them adept at handling uncertainties and parameter variations. They effectively govern fractional and integer-order systems (Maâmar & Rachid, 2014), making them suitable for managing nonlinear systems like DC-DC converters (Cech & Schlegel, 2013). Given their attributes, this study embraces a FOPID controller for a DC-DC buck converter system. With its five parameters, the FOPID controller provides ample room for tuning, potentially resulting in highly stable DC-DC converter systems. Precise tuning of these parameters is paramount to meet design specifications such as robustness against parameter changes, improved overshoot, and settling time (Dastjerdi et al., 2019).

Literature reveals extensive exploration into parameter tuning for controllers using metaheuristic algorithms such as (HHO) (Izci et al., 2023), particle swarm optimization (PSO) (Demir & Demirok, 2023), hybrid whale optimization (HWO) algorithm (Hekimoğlu & Ekinci, 2020), Lévy flight distribution (LFD) (Izci et al., 2022b), artificial ecosystem-based optimization (AEO) (Izci et al., 2022c), and genetic algorithm (GA) (Ortatepe, 2023). While HHO offers high accuracy in parameter optimization, it can stagnate in local search spaces. PSO is straightforward and resource-efficient. It suffers from premature convergence and local trapping. HWO excels in providing effective solutions but demands substantial computational power. LFD efficiently handles constrained search spaces but can get stuck in local solutions. AEO is powerful yet tends to be trapped in local minima.

The positive outcomes demonstrated by metaheuristic algorithms in fine-tuning controller parameters for regulating the buck converter system, as evidenced in the studies mentioned above, fostered the adoption of a newly introduced optimization technique known as the CSA (Feng et al., 2021). This study introduces an enhanced version incorporating OBL to improve exploration and leverage PS technique for better local optimization within CSA. This algorithm streamlines the design of a FOPID controller for a buck converter system, delivering improved efficiency, robustness, and stability.

**Contributions**

• An innovative hybrid metaheuristic algorithm has been developed by enhancing the CSA algorithm with OBL and PS. This enhancement effectively elevates the original CSA's exploration and exploitation capabilities.

• The supremacy of the newly proposed algorithm over CSA, HHO, and GA has been established via statistical boxplot and convergence response analyses.

• The OCSAPS algorithm was skillfully applied to fine-tune the parameters of a FOPID controller in a DC-DC buck converter system. An array of tests were conducted to showcase the superior performance of the OCSAPS-driven FOPID-controlled buck converter system. These tests encompassed evaluations of transient and frequency responses, a comparison of diverse performance metrics, and a robustness analysis.

• Moreover, a comparison was executed between the proposed approach and six other methodologies documented in existing literature. These methodologies were utilized for controlling DC-DC buck converter systems with FOPID controllers, focusing on both transient and frequency responses. This examination yet again underscored the preeminence of the OCSAPS algorithm.

## 2. MATERIAL AND METHOD

### 2.1. Cooperation Search Algorithm

The CSA is rooted in a company's core operational principle of keeping pace with a changing world, enhancing efficiency, and striving for excellence (Feng et al., 2021). To achieve these objectives, continuous enhancement of knowledge, experience, and productivity is required from all tiers of the organization. This involves sharing wisdom among each other and replacing underperforming staff with more capable individuals. The pivotal factor in attaining the mentioned objectives is effective collaboration between teams. Notably, even the highest-ranking executives can be substituted with talented and motivated newcomers if it serves the company's betterment.

The algorithm embodies problem optimization through staff members and teams. It compares problem fitness to staff performance, with executive managers and the board of directors symbolizing different solution levels. The algorithm employs three operators within the company for solution enhancement.The steps outlining the operational mechanism of the CSA algorithm are as follows:

***Team building phase*:** Here, all team members are chosen randomly using Eq. (1). After evaluating the accomplishments of all solutions, a set of M∈[1, *I*] promising solutions is picked from the initial batch to form the higher-ranking set.

$$x_{i,j}^{k} = \emptyset\left(\underline{x}_j, \bar{x}_j\right), i \in [1, I], j \in [1, J], k = 1 \tag{1}$$

where $x_{i,j}^{k}$ represents the $j^{th}$ value of the $i^{th}$ solution during the $k^{th}$ cycle. *I* denotes the solutions count within the present batch, while *J* signifies the number of variables that align with the optimization problem's dimension. Additionally, $\emptyset(L, U)$ refers to the function that generates a uniformly distributed random number within the range of $[L, U]$, where *L* and *U* denote the lower and upper constraints of the optimization variables, respectively.

***Team communication operator***: Each staff member can acquire fresh insights by exchanging knowledge with higher-ups, the board of directors, and supervisors. As indicated in Eq. (2), the communication process is divided into three segments: *A* stands for the chairperson's intellectual capacity, *B* denotes the cumulative knowledge retained by the board of directors, and *C* represents the combined intelligence held by the board of supervisors. The chairperson's selection is made arbitrarily from among the board of directors to replicate the rotational mechanism. Simultaneously, the values of *B* and *C* are calculated using identical positional information granted to all members of the board of directors and supervisors.

$$u_{i,j}^{k+1} = x_{i,j}^{k} + A_{i,j}^{k} + B_{i,j}^{k} + C_{i,j}^{k}, i \in [1, I], j \in [1, J], k \in [1, K] \tag{2}$$

$$A_{i,j}^{k} = \log\left(1/\emptyset(0,1)\right).\left(gbest_{m,j}^{k} - x_{i,j}^{k}\right) \tag{3}$$

$$B_{i,j}^{k} = \alpha.\emptyset(0,1).\left[\frac{1}{M}\sum_{m=1}^{M} gbest_{m,j}^{k} - x_{i,j}^{k}\right] \quad (4)$$

$$C_{i,j}^{k} = \beta.\emptyset(0,1).\left[\frac{1}{I}\sum_{i=1}^{I} pbest_{i,j}^{k} - x_{i,j}^{k}\right] \quad (5)$$

where $u_{i,j}^{k+1}$ signifies the $j^{th}$ value within the $i^{th}$ group solution during the $(k+1)^{th}$ cycle. The $j^{th}$ value of the $i^{th}$ personal best-known solution at the $k^{th}$ cycle is represented by $pbest_{i,j}^{k}$. Similarly, $gbest_{m,j}^{k}$ stands for the $j^{th}$ value within the global best-known solution of the $m^{th}$ instance, from the beginning until the $k^{th}$ cycle. The value of $m$ is randomly selected from the set $\{1,2,\dots,M\}$. Knowledge acquired from the chairman is indicated as $A_{i,j}^{k}$. The learning factors $\alpha$ and $\beta$ are used to fine-tune the influence of $B_{i,j}^{k}$ and $C_{i,j}^{k}$, respectively. $B_{i,j}^{k}$ corresponds to the average knowledge derived from the M best-known solutions achieved thus far over a wide range, while $C_{i,j}^{k}$ pertains to the personal best-known solutions of $I$ instances.

The computational coefficients (α, β, and M) are assigned the values 0.1, 0.15, and 3, respectively, in alignment with the original paper introducing the CSA algorithm (Feng et al., 2021).

***Reflective learning operator:*** In addition to gaining insights from the top-performing candidate solutions, the staff also has the opportunity to access novel information by consolidating its expertise in the opposite direction, as detailed in the equations below.

$$v_{i,j}^{k+1} = \begin{cases} r_{i,j}^{k+1} & if\left(u_{i,j}^{k+1} \geq c_j\right) \\ p_{i,j}^{k+1} & if\left(u_{i,j}^{k+1} < c_j\right) \end{cases}, i \in [1,I], j \in [1,J], k \in [1,K] \quad (6)$$

$$r_{i,j}^{k+1} = \begin{cases} \emptyset\left(\bar{x}_j + \underline{x}_j - u_{i,j}^{k+1}, c_j\right) & if\left(\left|u_{i,j}^{k+1} - c_j\right| < \emptyset(0,1).\left|\bar{x}_j - \underline{x}_j\right|\right) \\ \emptyset\left(\underline{x}_j, \bar{x}_j + \underline{x}_j - u_{i,j}^{k+1}\right) & \text{otherwise} \end{cases} \quad (7)$$

$$p_{i,j}^{k+1} = \begin{cases} \emptyset\left(c_j, \bar{x}_j + \underline{x}_j - u_{i,j}^{k+1}\right) & if\left(\left|u_{i,j}^{k+1} - c_j\right| < \emptyset(0,1).\left|\bar{x}_j - \underline{x}_j\right|\right) \\ \emptyset\left(\bar{x}_j + \underline{x}_j - u_{i,j}^{k+1}, \bar{x}_j\right) & \text{otherwise} \end{cases} \quad (8)$$

$$c_j = \left(\bar{x}_j + \underline{x}_j\right).0.5 \quad (9)$$

where $v_{i,j}^{k+1}$ is the $j^{th}$ value of the $i^{th}$ reflective solution at the $(k+1)^{th}$ cycle.

***Internal competition operator:*** The team consistently retains staff members exhibiting superior performance, thereby facilitating a gradual improvement in their competitive edge within the market. This preservation is ensured through the following expression.

$$x_{i,j}^{k+1} = \begin{cases} u_{i,j}^{k+1} & if\left(F\left(\boldsymbol{u}_i^{k+1}\right) \leq F\left(\boldsymbol{v}_i^{k+1}\right)\right) \\ v_{i,j}^{k+1} & if\left(F\left(\boldsymbol{u}_i^{k+1}\right) > F\left(\boldsymbol{v}_i^{k+1}\right)\right) \end{cases}, i \in [1,I], j \in [1,J], k \in [1,K] \quad (10)$$

where $F(\boldsymbol{x})$ represents the fitness value of the solution $\boldsymbol{x}$.

Pseudo code of the CSA can be observed in Algorithm 1. Here, the algorithm initiates by establishing the population size, defining the applicable boundaries, and initializing the iteration count. Subsequently, the designated objective function, outlined in section 4, is specified. The initial candidates are generated randomly, from which the initial solutions are derived. Key positions, including the personal best position, are determined

by utilizing CSA's operators. It is at this juncture that the essential boundary verification procedure is implemented. Ultimately, the updated versions of global best and personal best solutions are ascertained by employing reflective learning and internal competition operators. The algorithm exports the global best-known solution upon reaching the maximum iteration count.

***Algorithm 1.*** *Pseudo Code of the CSA.*

**Initialize**

Define initial parameters and objective function.

Generate random population in the practicable space.

Calculate the fitness of the initial randomly generated solutions.

Set t = 0

Set max iteration

**while** t < max iteration **do**

**for** each solution in the population **do**

Apply team communication operator using Eqs. (3-5)

Calculate group solution $u_{i,j}$

Update the $u_{i,j}^{k+1}$ position.

Apply reflective learning operator.

**if** $\frac{\left|u_{i,j}^{k+1}-c_j\right|}{\left|\bar{x}_j-\underline{x}_j\right|} < \emptyset(0,1)$ **then**

Determine $r_{i,j}^{k+1}$ and $p_{i,j}^{k+1}$ according to Eq. (7) and (8).

**end if**

**if** $u_{i,j}^{k+1} \geq c_j$ **then**

Determine $v_{i,j}^{k+1}$ according to Eq. (6).

**end if**

Perform boundary check.

Apply internal competition operator.

**if** $F(\boldsymbol{u}_i^{k+1}) \leq F\left(\boldsymbol{v}_i^{k+1}\right)$ **then**

Determine $x_{i,j}^{k+1}$ according to Eq. (10).

**end if**

**end for**

Update the personal best-known solutions from the initial population.

Update the global best-known solutions.

Increment *t* by 1.

**if** t >= max_iteration **then**

Export the global best-known solution.

**end if**

**end while**

### 2.2. Opposition-Based Learning

OBL is a widely recognized methodology that bolsters the exploration capacities of metaheuristic algorithms, as detailed by Tizhoosh (2005). A set of potential positions is generated randomly to identify the optimal solution. However, when there's no prior information regarding the proximity of the initially chosen position *x* to the optimal solution, the journey towards reaching the desired best solution could be notably protracted. In cases where the initially selected solution appears to be distant from the optimal solution or is situated unfavorably, it becomes prudent to simultaneously explore all directions, or more effectively, the direction opposite to the current position – a notion that aligns logically. The fundamental premise of OBL revolves around approaching the optimal solution by concurrently considering both the original value of the current position *x* and its opposite position $\overline{x}$.

Consider *x* as a real number confined within the interval of $[L, U]$. In a one-dimensional spatial context, the term 'opposite' denoted as $\overline{x}$ is defined as follows:

$$\overline{x} = U + L - x \tag{11}$$

For *n*-dimensional space, consider $x_i \in [L_i, U_i]$, and $i = 1,2, \dots, n$. In this case, $\overline{x}$ is defined as follows,

$$\bar{x}_i = U_i + L_i - x_i \tag{12}$$

Upon the random generation or recent update of all *x* positions, the corresponding opposing positions $\overline{x}$ are concurrently computed. Subsequently, the fitness evaluation is performed for both groups of positions (*x* and $\overline{x}$), identifying the most optimal positions. This iterative process progressively narrows the proximity to the optimal solution with each iteration.

### 2.3. Pattern Search Algorithm

Pattern Search (PS) techniques involve identifying successful search point patterns from recent history and leveraging this knowledge to forecast potentially fruitful search points in forthcoming iterations. These methods fall within the purview of direct search techniques, encompassing algorithms like the Simplex algorithm (Torczon, 1997). In this context, the Multidirectional Search (MDS) algorithm, a variant of the pattern search approach, was introduced by Torczon (1989) to tackle unconstrained minimization problems. The MDS algorithm excels at pinpointing optimal solutions by maintaining the most promising prior vertex and simultaneously conducting line searches in various directions, thereby accumulating valuable exploratory data. The flowchart illustrating the PS algorithm is depicted in Figure 1.

In this algorithm, the procedure begins with selecting the initial simplex, denoted as $S_0$, alongside expansion and contraction factors μ and θ. In each iteration, a search is executed from the current best vertex $v_0^k$, along each of the 'n' directions established by the edges connected to $v_0^k$. The primary objective of this search is to identify a fresh vertex boasting a function value lower than that of $v_0^k$. The algorithm proceeds with the reflection step if such a vertex is located. If not, it proceeds with the contraction step. During contraction, the algorithm continues until the condition $f(c_i^k) < f(v_0^k)$ is met. At this juncture, the current vertex is swapped with $c_i^k$, which exhibits a lower function value.

Conversely, in the expansion step, the algorithm computes $f(e_i^k)$ and compares it with $f(c_i^k)$. Depending on the outcome of this comparison, the algorithm decides to replace $v_i^k$ with either the expansion vertex $e_i^k$ or the reflection vertex $r_i^k$. The parameters θ, ρ, and μ, governing the lengths of the steps relative to the original simplex edges, play a pivotal role in these steps. For this implementation, θ, ρ, and μ, values are assigned as 0.5, 1, and 2, respectively, as in (Hekimoğlu, 2023). Additionally, a tolerance value crucial for algorithm termination and an initial step size required for generating the first simplex and are set to $10^{-5}$ and 0.05, respectively (Hekimoğlu, 2023).

Termination of the PS algorithm transpires either when the iteration count equals the stipulated maximum iteration count (set at 50 in this scenario) or when the difference between the worst and best solutions, referred to as the "distance," becomes smaller than the tolerance value.

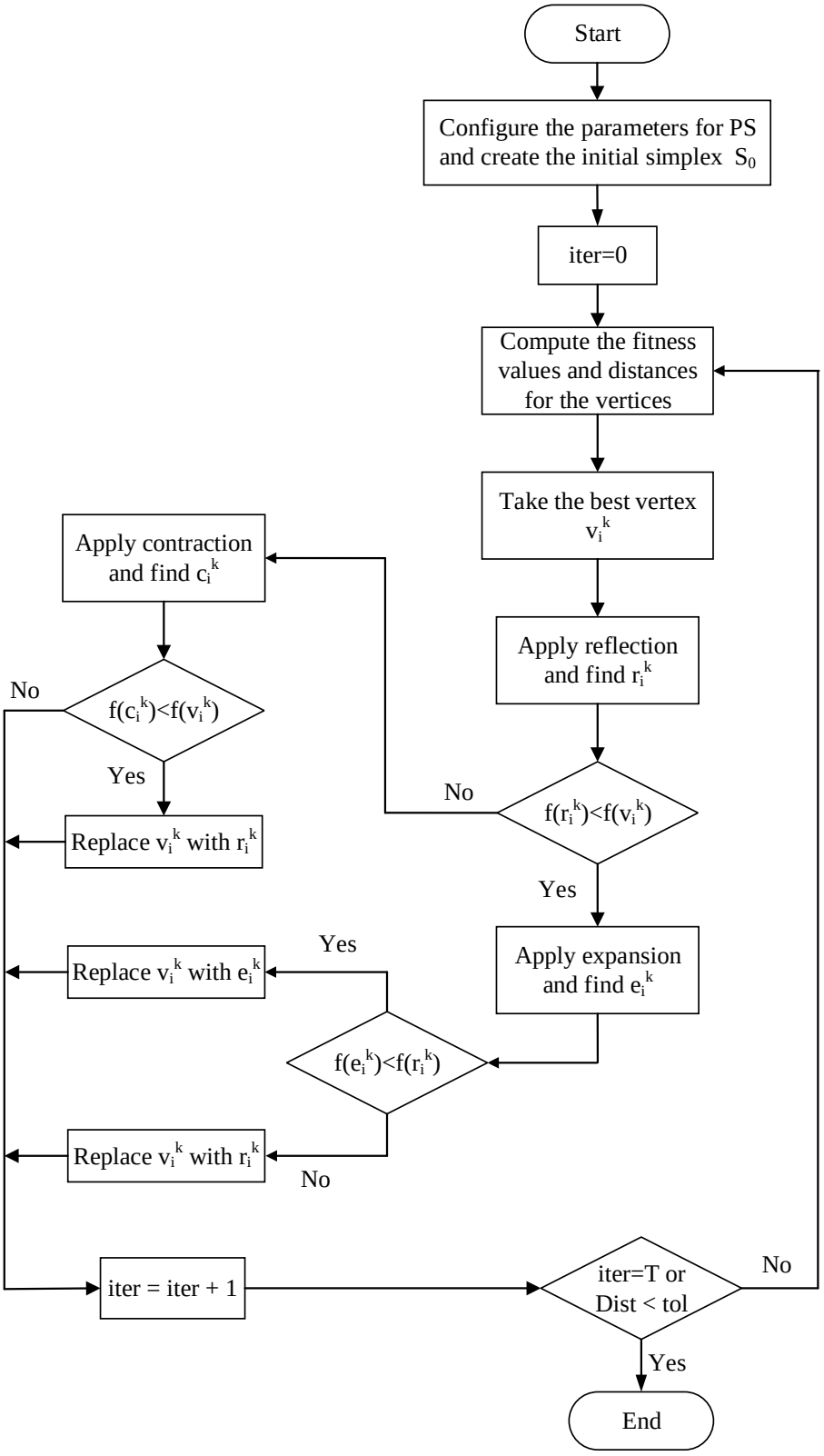


***Figure 1.*** *Flowchart of PS algorithm.*

### 2.4. Proposed OCSAPS Algorithm

While CSA exhibits superior overall performance compared to various traditional evolutionary algorithms (Feng et al., 2021), it's important to note that certain limitations are highlighted in (Feng et al., 2022). These limitations signify potential areas for enhancement. In the CSA approach, the reduction in staff variation gradually occurs over iterations, which might lead to premature convergence issues during the global search phase (Feng et al., 2022). To address this concern, an effective strategy involves integrating the OBL mechanism into CSA.

In the proposed hybrid algorithm named OCSAPS, this OBL mechanism introduces the capability to explore opposite directions within the global search space. This enhancement subsequently heightens the likelihood of discovering improved local search regions. Additionally, the proposed approach incorporates the PS algorithm to enhance its exploitation capabilities further. A visual representation of the OCSAPS algorithm's process can be found in Figure 2.

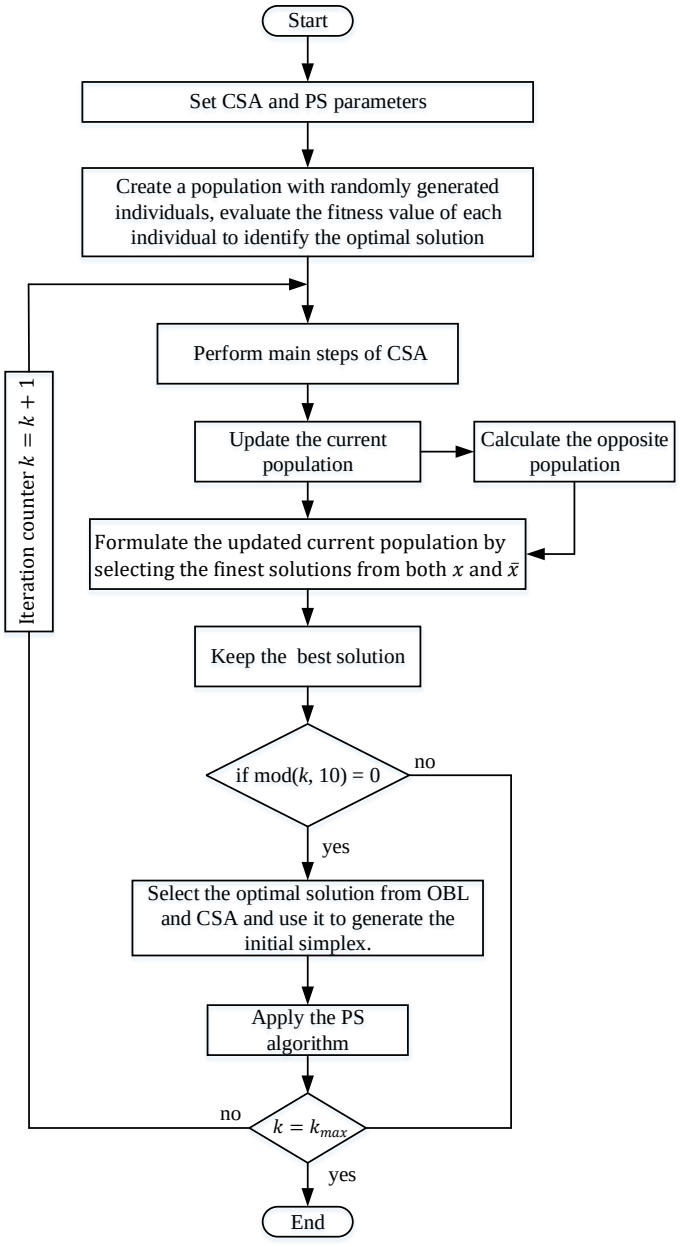


***Figure 2.*** *Flowchart of the proposed OCSAPS algorithm.*

## 3. BUCK CONVERTER SYSTEM WITH FOPID CONTROLLER

### 3.1. Mathematical Model of the Buck Converter

The DC-DC buck converter functions as a time-variant nonlinear switching circuit. Given its inherent nonlinearity, deriving a linearized model becomes imperative when designing a linear controller. Circuit or state-space averaging techniques are typically employed to achieve this linearized model (Erickson & Maksimović, 2000). The circuit diagram for the DC-DC buck converter is depicted in Figure 3.

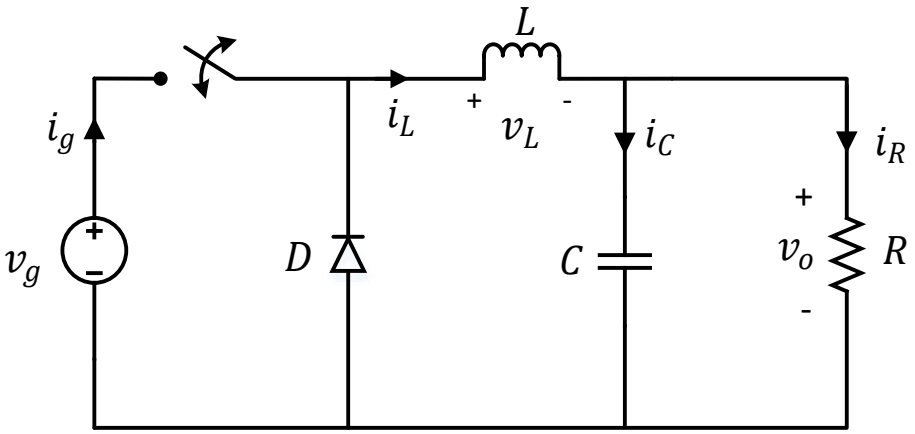


***Figure 3****. DC-DC buck converter.*

In the pursuit of linearization, a method called the switching signal-flow graph (SSFG) (Smedley & Cuk, 1994), based on state-space averaging, is utilized. This approach facilitates the computation of small-signal transfer functions required for controller design. The SSFG method employs visual representation to simplify deriving small-signal models for switching converters. The SSFG for the DC-DC buck converter is presented in Figure 4.

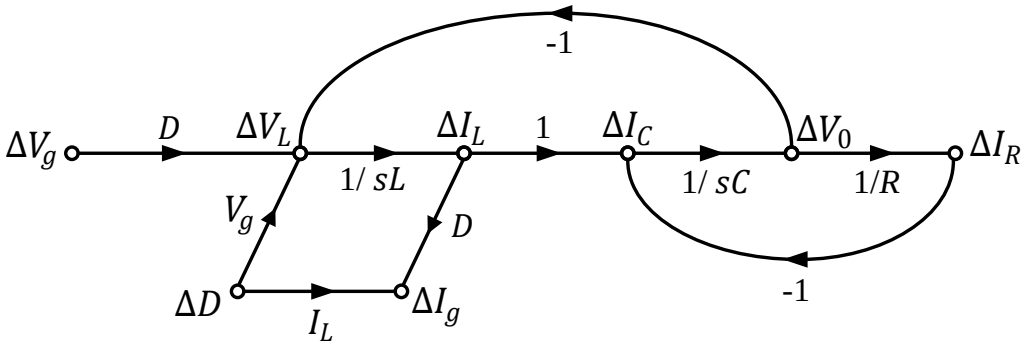


***Figure 4.*** *Small-signal model of DC-DC buck converter with SSFG method.*

Eq. (15) gives the transfer function from control to output, which stems from the small-signal model of the buck converter illustrated in Figure 4.

$$G_{vd}(s) = \frac{\Delta V_o(s)}{\Delta D(s)} = \frac{V_g/LC}{s^2 + s/RC + 1/LC} \tag{15}$$

where $V_g$ stands for the input voltage, $D$ denotes the duty cycle, $L$ signifies the inductance, $C$ represents the capacitance, and $R$ denotes the load resistance. The step response of the open-loop buck converter, employing the parameters detailed in Table 1, is illustrated in Figure 5.

***Table 1.*** *Buck converter parameters.*

| Parameters | Values |
|---|---|
| $V_g$ | 36 V |
| $D$ | 1/3 |
| $V_{ref}$ | 12 V |
| $L$ | 1 mH |
| $C$ | 100 µF |
| $R$ | 6 Ω |
| $f$ | 40 kHz |

A brief examination of Figure 5 immediately reveals that the step response of the buck converter, lacking a controller, falls short of the desired ideal behavior. It displays significant overshoot, an extended settling period, and a prolonged duration to attain a stable state. Integrating a controller into the buck converter system becomes imperative to rectify these unfavorable traits within the converter's transient response. In this instance, a fractional order proportional integral derivative (FOPID) controller will be implemented to enhance the aforementioned transient response attributes.

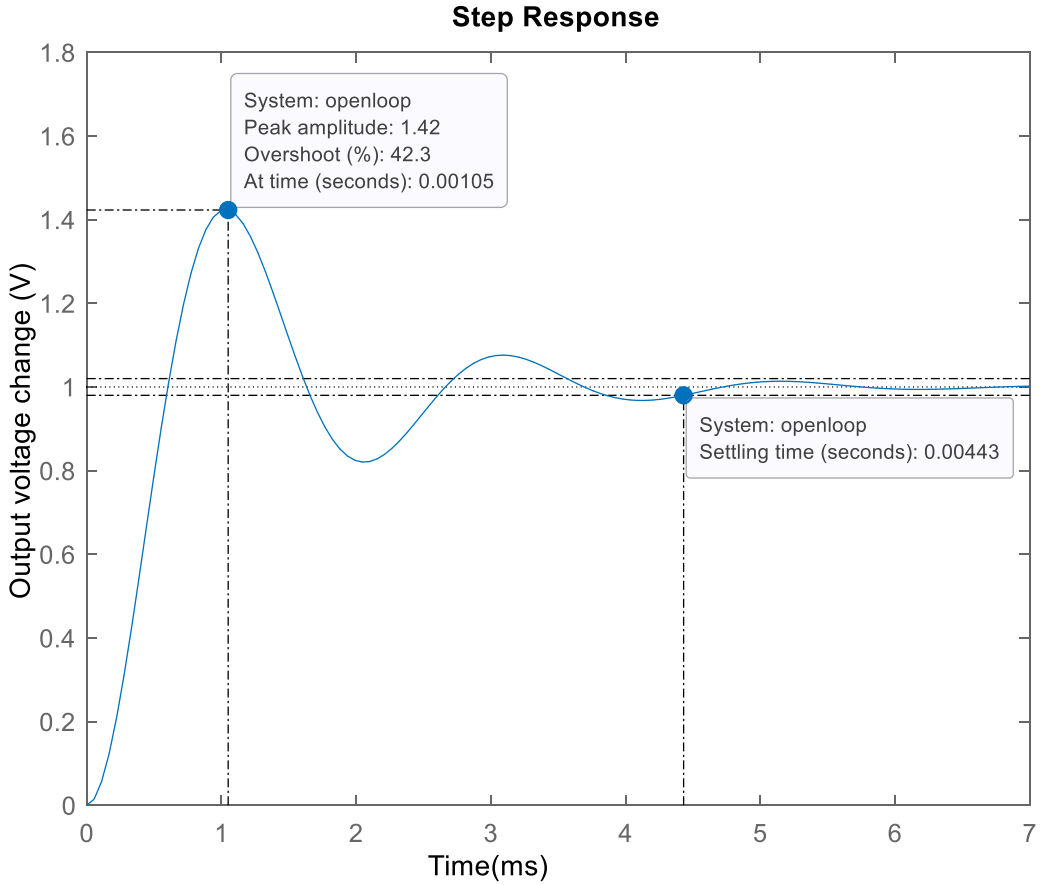


***Figure 5.*** *Open-loop response of the buck converter system.*

### 3.2. Fractional Order PID (FOPID) Controller

The FOPID controller represents a broader version of the conventional PID controller, specifically designed to accommodate fractional orders. It was initially introduced by Podlubny (1999). This controller incorporates two auxiliary parameters, namely λ and μ, which correspond to the fractional orders associated with the integral and derivative terms, respectively. These parameters introduce increased versatility and enhanced robustness. Fractional-order controllers, including fractional PID controllers, are acknowledged for delivering superior control performance in nonlinear systems featuring intricate dynamics, surpassing the capabilities of conventional integer-order controllers, as demonstrated in (Martinez-Patiño et al., 2023). They additionally provide enhanced adaptability when fine-tuning the controller's response to diverse system types attributed to the fractional derivative and proportional parameters at their disposal (Mohd Tumari et al., 2023). The transfer function of the FOPID controller is given in Eq. (16).

$$K_p + \frac{K_i}{s^{\lambda}} + K_d s^{\mu} \tag{16}$$

where $K_p$, $K_i$, and $K_d$ represent the proportional, integral, and derivative gains, respectively. Compared to a PID controller, FOPID incorporates two supplementary parameters, offering enhanced precision in fine-tuning the controller's behavior and thereby bolstering the system's overall stability. Nonetheless, including these additional parameters demands a more intricate parameter adjustment process than a conventional PID controller. Moreover, implementing FOPID controllers presents specific challenges, such as memory requirements. As non-integer integrators and differentiators necessitate an infinite memory capacity, conventional methods are inadequate for executing non-integer order controllers (Li & Zhao, 2015). Consequently, the efficient realization of FOPID controllers hinges on employing appropriate approximations. In the present scenario, the chosen approach is Oustaloup's approximation method (Oustaloup et al., 2000), which addresses the need for effective FOPID controller design.

Denote the frequency range as $(\omega_b, \omega_h)$ where $N$ represents the degree and $2N+1$ stands for the order of the approximation. The methodology proposed by Oustaloup for $s^{\alpha}$, where $0 < \alpha < 1$, is derived and detailed in Equations (16) and (17).

$$G_f(s) = K \prod_{k=-N}^{N} \frac{s + \omega_k'}{s + \omega_k} \tag{16}$$

$$\omega_k' = \omega_b \left(\frac{\omega_h}{\omega_b}\right)^{\frac{k+N+\frac{1}{2}(1-\alpha)}{2N+1}}, \omega_k = \omega_b \left(\frac{\omega_h}{\omega_b}\right)^{\frac{k+N+\frac{1}{2}(1+\alpha)}{2N+1}}, K = \omega_h^{\alpha} \tag{17}$$

where $K$ denotes the DC gain of the filter, $\omega_k'$ and $\omega_k$ represent the frequencies associated with the zeros and poles, respectively. For this study, an 11$^{th}$ order Oustaloup's approximation was adopted with $N$ set at 5. This approximation was applied within the frequency range of $(10^{-3}, 10^{3})$ rad/s. As such, the lower and upper boundaries of this approximation, designated as $\omega_b$ and $\omega_h$, respectively, were established as $10^{-3}$ rad/s and $10^{3}$ rad/s.

### 3.3. FOPID-Controlled Buck Converter System

Figure 6 illustrates the block diagram incorporating the FOPID controller to the buck converter. Additionally, the closed-loop transfer function for the buck converter system, enhanced by the FOPID controller, is defined by Eq. (18).

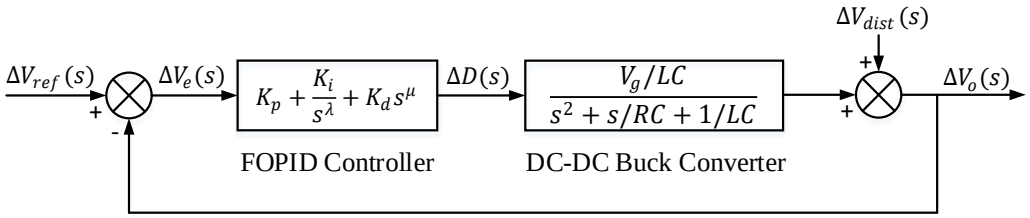


***Figure 6.*** *FOPID-controlled buck converter system*

$$\frac{\Delta V_o(s)}{\Delta V_{ref}(s)} = \frac{G_{FOPID}(s)G_{Buck}(s)}{1 + G_{FOPID}(s)G_{Buck}(s)}, \Delta V_{dist}(s) = 0 \tag{18}$$

where $\Delta V_o(s)$, $\Delta V_{ref}(s)$, and $\Delta V_{dist}(s)$ denote changes in the output voltage, reference voltage, and disturbance voltage, respectively. The closed-loop transfer function for the FOPID-controlled buck converter is given in Eq. (19).

$$\frac{\Delta V_o(s)}{\Delta V_{ref}(s)} = \frac{\left(K_p s^\lambda + K_i + K_d s^{\lambda+\mu}\right)V_g/LC}{s^\lambda(s^2 + s/RC + 1/LC) + \left(K_p s^\lambda + K_i + K_d s^{\lambda+\mu}\right)V_g/LC} \tag{19}$$

The ranges within which the FOPID parameters are employed for this study are specified in Equation (20).

$$\begin{gathered} 1 \le K_p \le 50 \\ 0.01 \le K_i \le 10 \\ 0.001 \le K_d \le 0.02 \\ 0 \le \lambda, \mu \le 2 \end{gathered} \tag{20}$$

## 4. PERFORMANCE INDEX AND OBJECTIVE FUNCTION

The paramount objective in designing a control system is minimizing the error between the output and the reference value. This pursuit significantly contributes to the system's robustness and overall stability. Consequently, integral performance metrics are widely adopted to evaluate the performance of a controller (Boudjehem & Boudjehem, 2016). Various integral performance metrics have recently been applied to craft fractional-order control systems (Das et al., 2012; Pan & Liu, 2016; Eshaghi & Tavazoei, 2023; Ranjan & Mehta, 2023). From this assortment of performance metrics, the integral absolute error (IAE) will be utilized in this study to minimize the error mentioned above and subsequently enhance the output voltage of the buck converter.

The choice to utilize the IAE objective function arises from the observation that implementing this approach during the algorithmic process for determining the necessary parameters of the FOPID controller results in the most favorable outcomes.

$$IAE = \int_0^T |e(t)|\, dt \tag{21}$$

Eq. (21) provides the integral formulation of the aforementioned performance index. In this equation, $e(t)$ signifies the error arising from subtracting the closed-loop buck converter system's output voltage from its reference voltage. The simulation duration, denoted as *T*, is $5\text{x}10^{-6}$ seconds.

## 5. IMPLEMENTATION OF OCSAPS TO BUCK CONVERTER SYSTEM

Figure 7 presents a block diagram that depicts the integration of OCSAPS into the buck converter system. The diagram reveals that the FOPID controller parameters derived from OCSAPS dictate the buck converter system's output voltage. Subsequently, the output voltage is compared with the reference voltage, and the

objective is to minimize the error between these values to achieve the targeted system performance. The objective function plays a crucial role in minimizing this error, aiming to bring the comparison outcome as close to zero as possible.

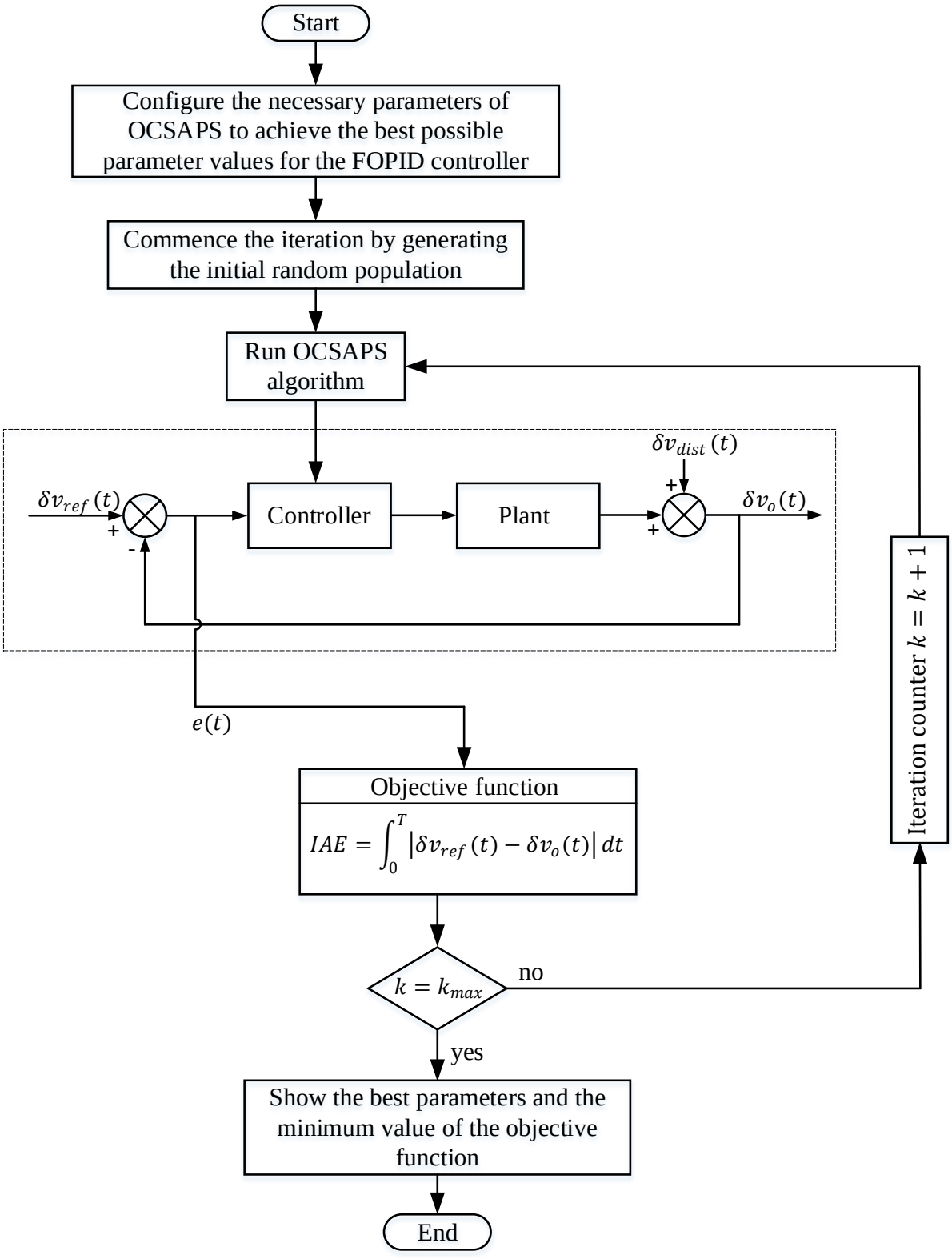


***Figure 7.*** *Application of the OCSAPS algorithm to the FOPID-controlled buck converter system.*

## 6. SIMULATION RESULTS AND DISCUSSION

The proposed OCSAPS algorithm underwent a comparative analysis against several other algorithms: the original CSA (Feng et al., 2021) and two highly successful algorithms, HHO and GA, in controlling the buck converter system with the FOPID controller. The algorithms were executed with uniform settings: a maximum iteration count of 30 and 25 runs. Evaluations were conducted on a desktop computer equipped with an Intel Core i5 3.30 GHz processor and 16 GB of RAM. MATLAB software was the chosen platform for conducting the analyses.

### 6.1. Statistical Boxplot Analysis

A visual representation of the data distribution is presented through boxplot analysis for OCSAPS, CSA, HHO, and GA algorithms, offering readers a straightforward initial assessment. Statistical metrics encompassing best, mean, median variance, standard deviation, and worst (detailed in Table 2) underscore that the OCSAPS algorithm outperforms the original CSA and the other compared algorithms. The results depicted in Figure 8 illustrate how the OCSAPS algorithm attains notably lower values in terms of upper quartile, lower quartile, maximum score, median, and minimum score compared to the mentioned algorithms. This pattern suggests the superiority of the proposed OCSAPS approach over the other compared algorithms.

***Table 2.*** *Statistical results of IAE objective function for the compared algorithms.*

| Statistical metric | OCSAPS | CSA | HHO | GA |
|---|---|---|---|---|
| Best | $\mathbf{1.10979x10^{-7}}$ | $1.15239x10^{-7}$ | $1.14736x10^{-7}$ | $1.18042x10^{-7}$ |
| Mean | $\mathbf{1.11789x10^{-7}}$ | $1.43149x10^{-7}$ | $3.18071x10^{-7}$ | $3.21815x10^{-7}$ |
| Median | $\mathbf{1.11222x10^{-7}}$ | $1.39617x10^{-7}$ | $1.44622x10^{-7}$ | $2.39439x10^{-7}$ |
| Variance | $\mathbf{1.27131x10^{-18}}$ | $2.62815x10^{-16}$ | $6.28873x10^{-13}$ | $5.68841x10^{-14}$ |
| Standard deviation | $\mathbf{1.12753x10^{-9}}$ | $1.62116x10^{-8}$ | $7.93015x10^{-8}$ | $2.38504x10^{-7}$ |
| Worst | $\mathbf{1.14826x10^{-7}}$ | $1.85696x10^{-7}$ | $4.53744x10^{-6}$ | $1.06497x10^{-6}$ |

### 6.2. Convergence Response

In Figure 9, the convergence extent of the objective function values achieved through the execution of the OCSAPS, CSA, HHO, and GA are displayed. It's important to note that due to the inherent stochastic nature of metaheuristic algorithms, not all runs produce identical outcomes. Accordingly, among the nearly 30 iterations of these algorithms, it becomes apparent that CSA, HHO, and GA consistently deliver less favorable outcomes than OCSAPS. This observation is substantiated by the insights derived from the statistical boxplot analysis depicted in Figure 8.

The data presented in Figure 9 underscores the significant impact of incorporating the OBL and pattern search techniques into CSA, resulting in a substantial improvement in discovering superior solutions at an accelerated pace.

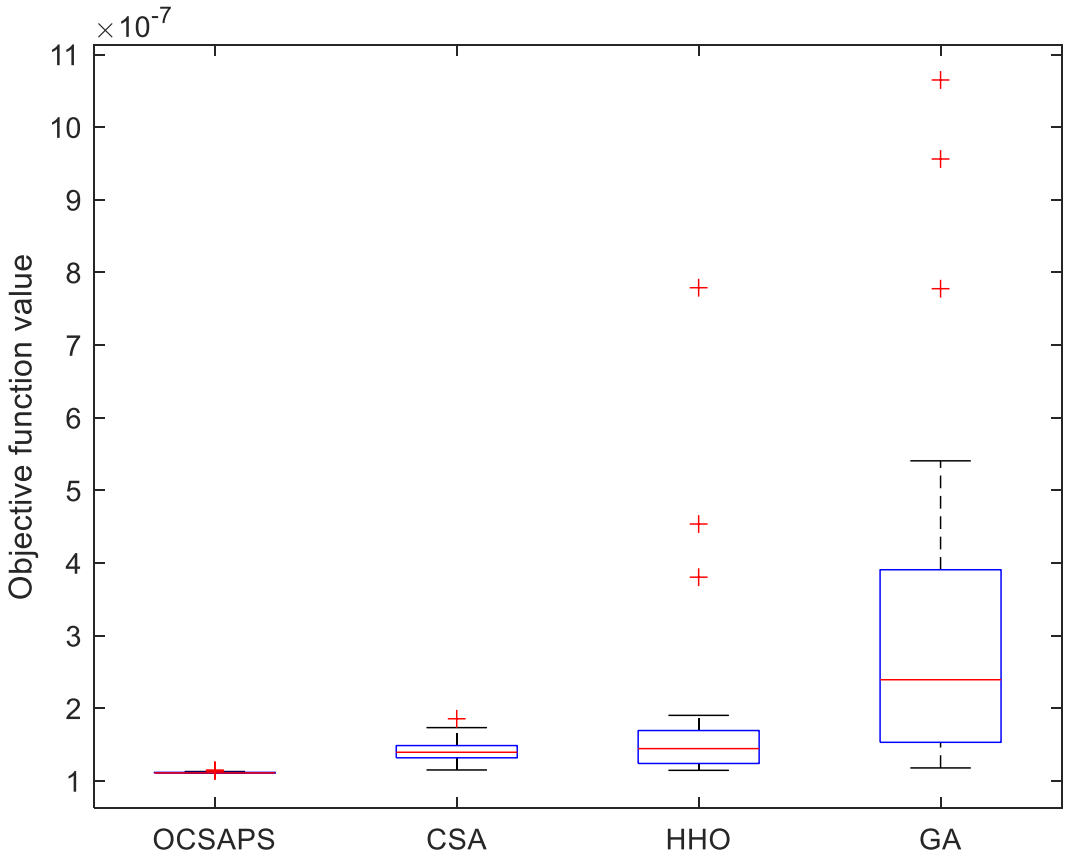


***Figure 8.*** *Comparison of the proposed OCSAPS, CSA, HHO, and GA in terms of boxplot analysis.*

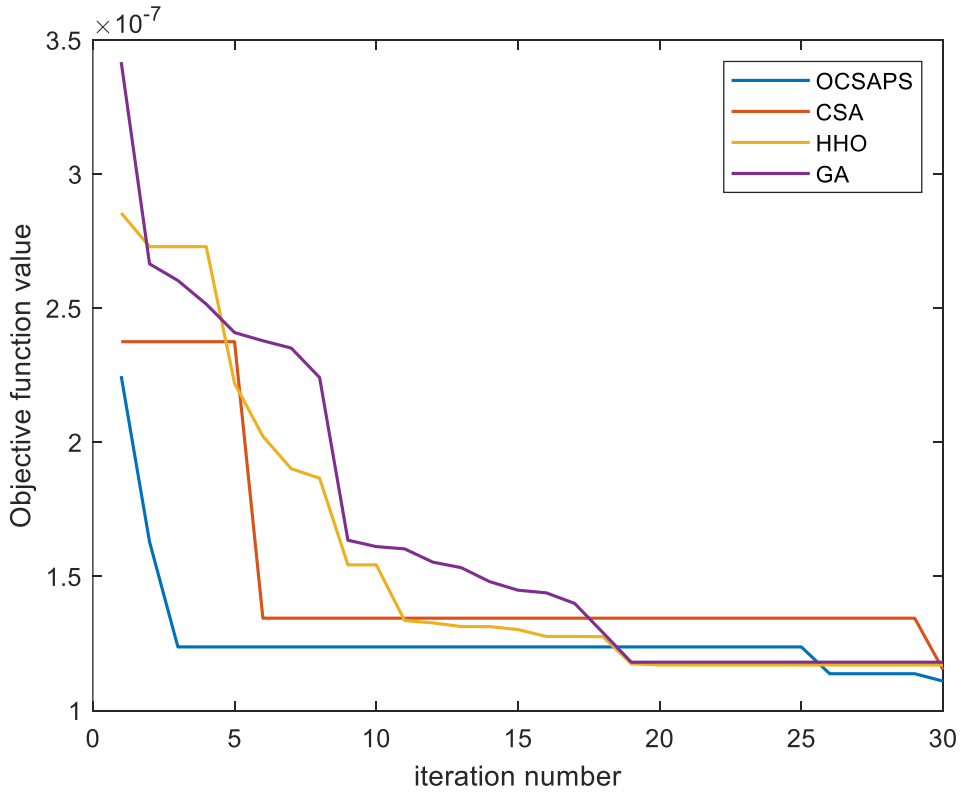


***Figure 9.*** *Comparison of the proposed OCSAPS, CSA, HHO, and GA in terms of convergence behavior.*

Table 3 presents the optimal FOPID controller parameters achieved through the optimization process for compared algorithms that govern the buck converter system. Additionally, employing these parameters, the closed-loop transfer functions of the integrated system have been calculated, as denoted by Eqs. (22), (23), (24), and (25).

***Table 3.*** *Optimal FOPID controller parameters of compared algorithms.*

| FOPID parameter | OCSAPS | CSA | HHO | GA |
|---|---|---|---|---|
| $K_p$ | 28.4424 | 32.4591 | 18.0622 | 28.5346 |
| $K_i$ | 9.3765 | 0.5960 | 1.6709 | 3.8269 |
| $K_d$ | 0.01 | 0.00841 | 0.009924 | 0.0097 |
| μ | 1.0522 | 1.0553 | 0.6094 | 0.2620 |
| λ | 1.1231 | 1.1146 | 1.0972 | 1.0959 |

$$\mathrm{G_{OCSAPS}}(s) = \frac{0.36s^{2.1753} + 1023.9s^{1.0522} + 337.55}{10^{-7}s^{3.0522} + 0.36s^{2.1753} + 0.0001667s^{2.0522} + 1024.9s^{1.0522} + 337.55} \tag{22}$$

$$\mathrm{G_{CSA}}(s) = \frac{0.30276s^{2.1699} + 1168.5s^{1.0553} + 21.456}{10^{-7}s^{3.0553} + 0.30276s^{2.1699} + 0.0001667s^{2.0553} + 1169.5s^{1.0553} + 21.456} \tag{23}$$

$$\mathrm{G_{HHO}}(s) = \frac{0.35726s^{1.7066} + 650.24s^{0.6094} + 60.152}{10^{-7}s^{2.6094} + 0.35726s^{1.7066} + 0.0001667s^{1.6094} + 651.24s^{0.6094} + 60.152} \tag{24}$$

$$\mathrm{G_{GA}}(s) = \frac{0.3492s^{1.3579} + 1027.2s^{0.262} + 137.77}{10^{-7}s^{2.262} + 0.3492s^{1.3579} + 0.0001667s^{1.262} + 1028.2s^{0.262} + 137.77} \tag{25}$$

### 6.3. Transient Response Analysis

Figure 10 illustrates a comparison of the unit step responses for the buck converter system employing different algorithms with FOPID controller. The comparison is conducted using the proposed OCSAPS, CSA, HHO, and GA algorithms. Additionally, a comparison of the transient response performance of systems based on these algorithms is presented in Table 4. Both the figure and the table collectively demonstrate that the FOPID-controlled buck converter system using the proposed OCSAPS algorithm exhibits the quickest rise time, settling time, and peak time compared to the other algorithms under consideration.

This observation implies that the FOPID-controlled buck converter system, utilizing the proposed OCSAPS algorithm, achieves superior operational efficiency compared to the algorithms mentioned earlier.

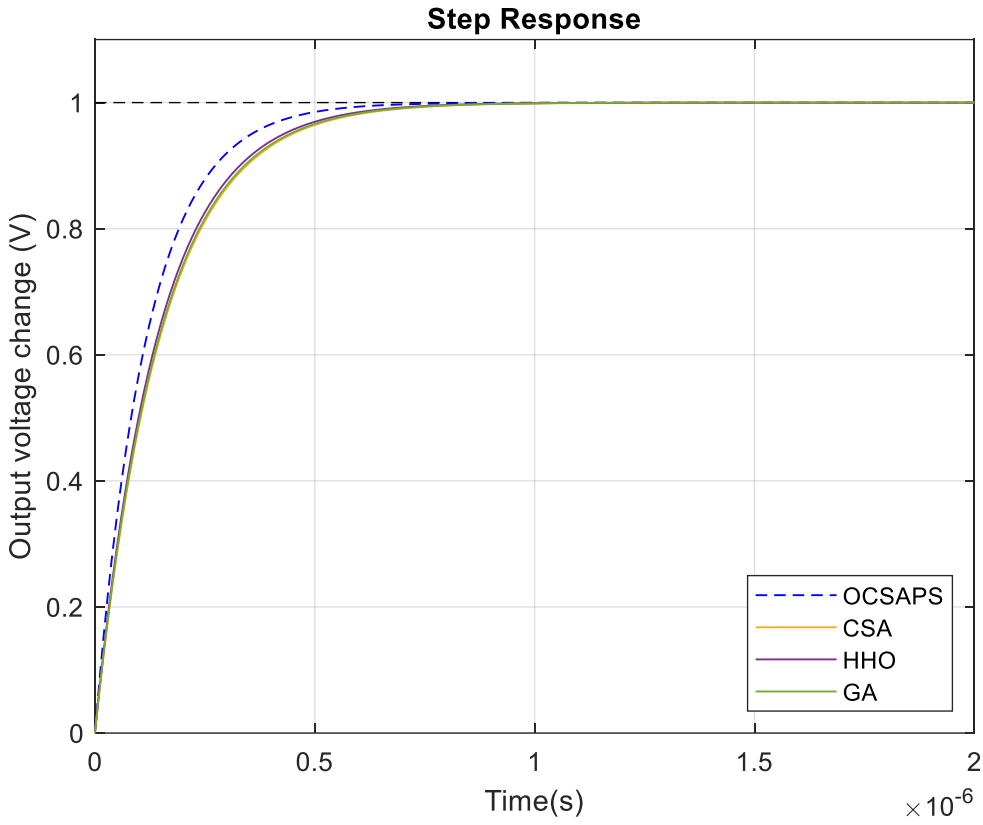


***Figure 10.*** *Transient response comparison of FOPID controllers for different algorithms.*

***Table 4.*** *Transient response metrics of compared algorithms.*

| Controller type | Maximum overshoot (%) | Rise time (s) | Settling time (s) | Peak time (s) |
|---|---|---|---|---|
| OCSAPS-FOPID | 0 | **$2.6081\text{x}10^{-7}$** | **$4.6467\text{x}10^{-7}$** | **$6.8863\text{x}10^{-7}$** |
| CSA-FOPID | 0 | $3.2880\text{x}10^{-7}$ | $5.8550\text{x}10^{-7}$ | $8.6839\text{x}10^{-7}$ |
| HHO-FOPID | 0 | $3.1434\text{x}10^{-7}$ | $5.6030\text{x}10^{-7}$ | $8.2980\text{x}10^{-7}$ |
| GA-FOPID | 0 | $3.2441\text{x}10^{-7}$ | $5.7781\text{x}10^{-7}$ | $8.5670\text{x}10^{-7}$ |

### 6.4. Frequency Response Analysis

Figure 11 illustrates the Bode plots for the buck converter system employing the OCSAPS algorithm proposed in this study. These plots are compared with those of the original CSA, HHO, and GA-based systems. In addition, Table 5 provides performance metrics in the frequency domain, including gain margin, phase margin, and bandwidth. The findings from the presented figure and table indicate that the system utilizing the proposed algorithm boasts a considerably broader bandwidth and phase margin than other systems mentioned. Consequently, the proposed algorithm-based system exhibits improved stability when compared against the other systems under comparison.

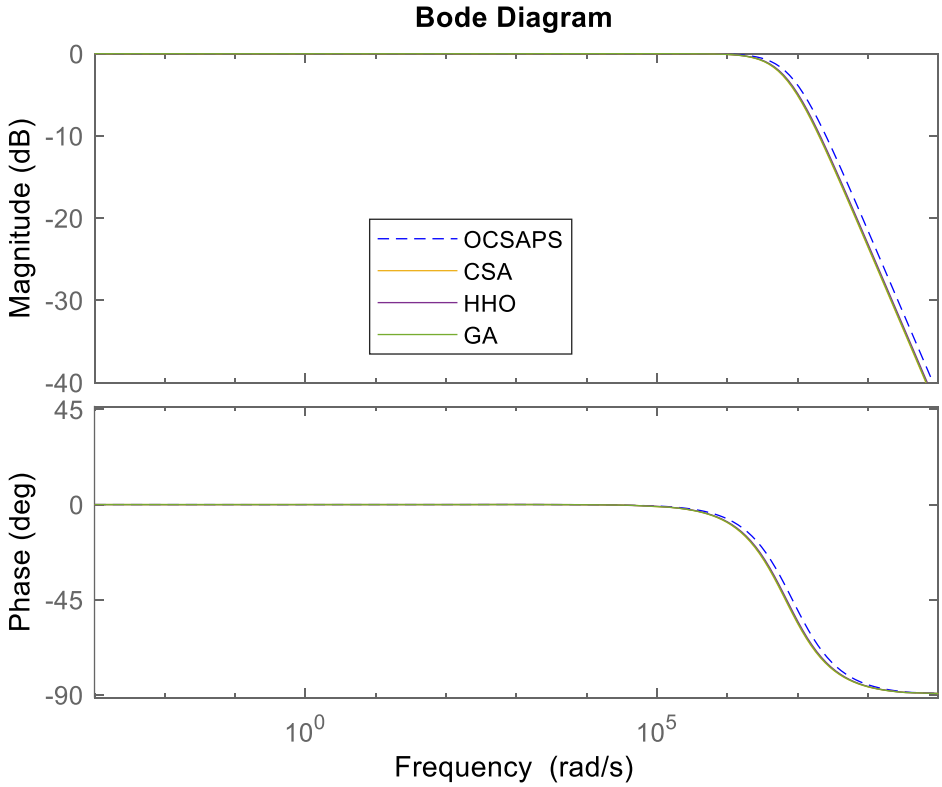


***Figure 11.*** *Closed-loop frequency responses of FOPID-controlled systems under comparison.*

***Table 5.*** *Comparison of frequency response metrics of different algorithms.*

| Controller type | Gain margin (dB) | Phase margin (deg) | Bandwidth (Hz) |
|---|---|---|---|
| OCSAPS-FOPID | **Inf.** | **89.9970** | **8.4051x10$^6$** |
| CSA-FOPID | **Inf.** | 89.9882 | 6.6660x10$^6$ |
| HHO-FOPID | **Inf.** | 1.1785 | 6.9774x10$^6$ |
| GA-FOPID | **Inf.** | 0.9419 | 6.7639x10$^6$ |

### 6.5. Comparison of Performance Indices

Other than the previously mentioned IAE presented in Eq. (21), several commonly employed performance measures exist. These include the integral of time-weighted squared error (ITSE), integral of time-weighted absolute error (ITAE), integral of squared error (ISE), and the time domain performance metric ZLG (Hekimoğlu, 2019), which was introduced by Gaing (2004). These metrics further highlight the exceptional performance of the proposed OCSAPS algorithm-based buck converter system. The formulations for these performance measures are provided in Eqs. (26), (27), (28), and (29) respectively.

$$ISE = \int_0^T \left(\delta v_{ref}(t) - \delta v_o(t)\right)^2 dt \tag{26}$$

$$ITAE = \int_0^T t\left|\delta v_{ref}(t) - \delta v_o(t)\right| dt \tag{27}$$

$$ITSE = \int_0^T t\left(\delta v_{ref}(t) - \delta v_o(t)\right)^2 dt \tag{28}$$

$$ZLG = (1 - e^{-\rho})\left(M_p + E_{ss}\right) + e^{-\rho}(T_s - T_r) \tag{29}$$

where $T$ represents the simulation duration, set at 5 microseconds, while $\delta v_{ref}$ signifies the change in reference voltage and $\delta v_o$ denotes the change in output voltage, the weighting coefficient is represented as $\rho$, $M_p$ stands for the maximum overshoot, $E_{ss}$ represents the steady-state error, $T_s$ indicates the settling time, and $T_r$ signifies the rise time. Minimizing these performance measures translates to enhanced robustness and stability for the buck converter system. Consequently, lower values correspond to heightened system stability. As shown in Table 6, the buck converter system based on the proposed OCSAPS algorithm boasts the smallest values across all the aforementioned performance measures. Once again, this underscores the system's superiority driven by the proposed algorithm.

***Table 6.*** *Performance indices of compared algorithms.*

| Controller type | ZLG | IAE | ISE | ITAE | ITSE |
|---|---|---|---|---|---|
| OCSAPS-FOPID | $\mathbf{2.1929x10^{-7}}$ | $\mathbf{1.1888x10^{-7}}$ | $\mathbf{5.9487x10^{-8}}$ | $\mathbf{1.4212x10^{-14}}$ | $\mathbf{3.5142x10^{-15}}$ |
| CSA-FOPID | $2.7182x10^{-7}$ | $1.4972x10^{-7}$ | $7.4941x10^{-8}$ | $2.2399x10^{-14}$ | $5.5912x10^{-15}$ |
| HHO-FOPID | $2.6165x10^{-7}$ | $1.4329x10^{-7}$ | $7.1637x10^{-8}$ | $2.0682x10^{-14}$ | $5.1082x10^{-15}$ |
| GA-FOPID | $2.6865x10^{-7}$ | $1.4776x10^{-7}$ | $7.3939x10^{-8}$ | $2.1853x10^{-14}$ | $5.4423x10^{-15}$ |

### 6.6. Robustness Analysis

A crucial aspect of a controller's effectiveness lies in its ability to withstand unforeseen scenarios, such as alterations in component values within the system due to environmental factors like temperature fluctuations, humidity changes, and gradual degradation over time. With this consideration in mind, variations in the inductor and capacitor values have been introduced in four distinct cases, outlined in Table 7, to assess the transient response characteristics of the system in response to the perturbations mentioned above. For comparison, the same changes in component values have been applied to the other three algorithm-based systems against which the proposed OCSAPS approach has been benchmarked so far.

Table 8 provides a comprehensive overview of the transient response metrics obtained by implementing said cases on the various algorithm-driven FOPID-controlled systems being evaluated. Across all instances, the buck converter system controlled by the proposed OCSAPS method consistently exhibits the shortest rise time, settling time, and peak time. Notice the robustness shortcomings of HHO in the case of increasing $C$ by 20% and of GA in the case of decreasing $L$ by 20 %. This illustrates that the proposed approach imparts greater robustness and stability to the buck converter system than other algorithm-based counterparts. These results further validate and reinforce the superiority of the proposed algorithm in this context.

***Table 7.*** *Impacts of altering system parameters on the transient response across different algorithms.*

| Case | Algorithm | Maximum overshoot (%) | Rise time (s) | Settling time (s) | Peak time (s) |
|---|---|---|---|---|---|
| Increasing *C* by %20 | OCSAPS | 0 | **$3.1294\text{x}10^{-7}$** | **$5.5743\text{x}10^{-7}$** | **$8.4051\text{x}10^{-7}$** |
| | CSA | 0 | $3.9451\text{x}10^{-7}$ | $7.0222\text{x}10^{-7}$ | $10.421\text{x}10^{-7}$ |
| | HHO | 0 | $1.7651\text{x}10^{-4}$ | $2.1623\text{x}10^{-4}$ | $2.2056\text{x}10^{-4}$ |
| | GA | 0 | $3.8924\text{x}10^{-7}$ | $6.9304\text{x}10^{-7}$ | $10.281\text{x}10^{-7}$ |
| Decreasing *C* by %20 | OCSAPS | 0 | **$2.0866\text{x}10^{-7}$** | **$3.7185\text{x}10^{-7}$** | **$5.5089\text{x}10^{-7}$** |
| | CSA | 0 | $2.6308\text{x}10^{-7}$ | $4.6866\text{x}10^{-7}$ | $6.9468\text{x}10^{-7}$ |
| | HHO | 0 | $2.5149\text{x}10^{-7}$ | $4.4387\text{x}10^{-7}$ | $6.6383\text{x}10^{-7}$ |
| | GA | 0 | $2.5957\text{x}10^{-7}$ | $4.6248\text{x}10^{-7}$ | $6.8533\text{x}10^{-7}$ |
| Increasing *L* by %20 | OCSAPS | 0 | **$3.1298\text{x}10^{-7}$** | **$5.5769\text{x}10^{-7}$** | **$8.2634\text{x}10^{-7}$** |
| | CSA | 0 | $3.9457\text{x}10^{-7}$ | $7.0261\text{x}10^{-7}$ | $10.421\text{x}10^{-7}$ |
| | HHO | 0 | $3.7724\text{x}10^{-7}$ | $6.7255\text{x}10^{-7}$ | $9.9574\text{x}10^{-7}$ |
| | GA | 0 | $3.8930\text{x}10^{-7}$ | $6.9342\text{x}10^{-7}$ | $10.280\text{x}10^{-7}$ |
| Decreasing *L* by %20 | OCSAPS | 0 | **$2.0864\text{x}10^{-7}$** | **$3.7167\text{x}10^{-7}$** | **$5.5091\text{x}10^{-7}$** |
| | CSA | 0 | $2.6034\text{x}10^{-7}$ | $4.6840\text{x}10^{-7}$ | $6.9471\text{x}10^{-7}$ |
| | HHO | 0 | $2.5146\text{x}10^{-7}$ | $4.4811\text{x}10^{-7}$ | $6.6386\text{x}10^{-7}$ |
| | GA | 0 | $2.1954\text{x}10^{-4}$ | $2.6894\text{x}10^{-4}$ | $2.7433\text{x}10^{-4}$ |

Apart from the effects of changes in component values on the output of the system, trajectory tracking performance has also been examined. Figure 12 provides performance comparison of different algorithms against output voltage change. At 2 ms and 4 ms, the output voltage has been changed by -25% and +25%, respectively, to see the trajectory tracking performance of the compared algorithms. Similar to Figure 10, the proposed approach-based controller performs better than the other algorithm-based controllers, which also validates its superior capability in terms of robustness.

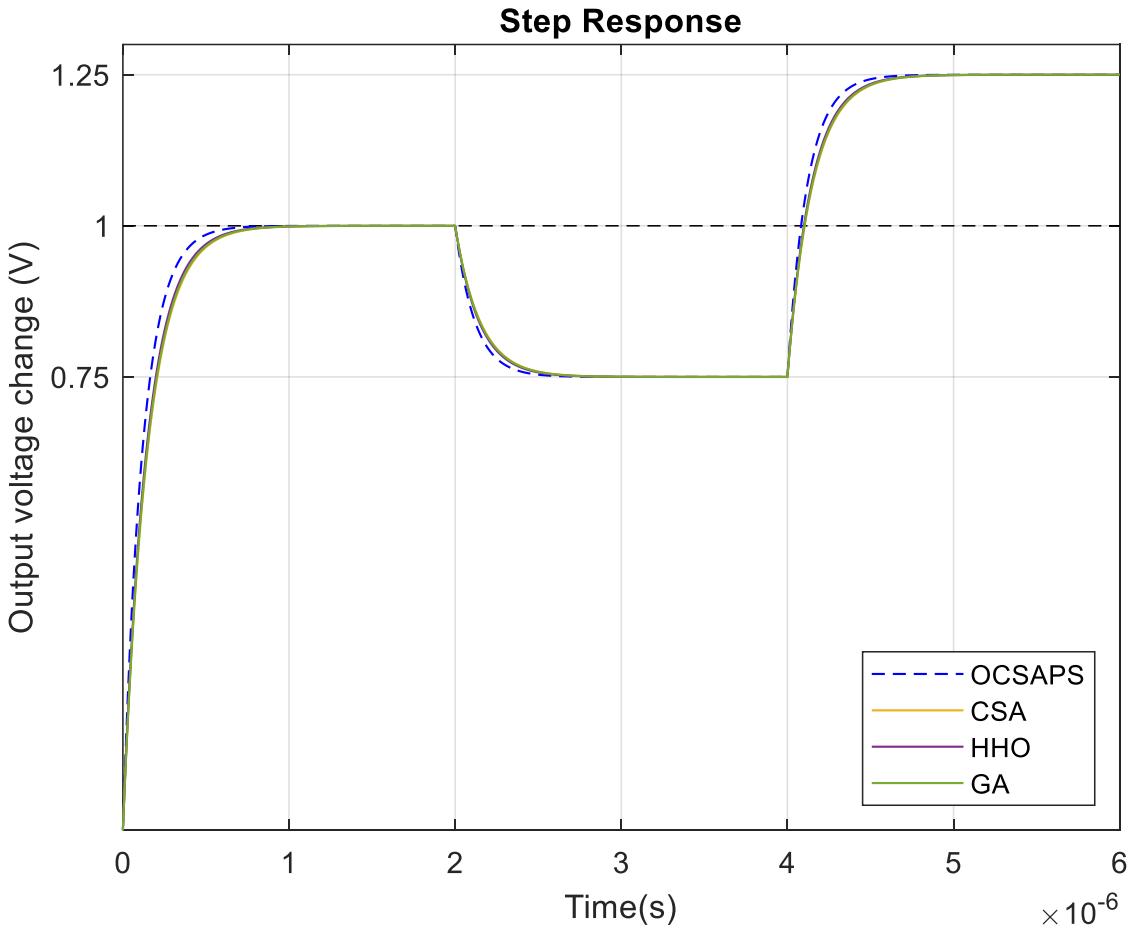


*Figure 12. Trajectory tracking comparison for different algorithms against output voltage change.*

### 6.7. Comparison with the Published Works

Numerous algorithms based on metaheuristic techniques can be found in existing literature. These algorithms aim to manage a buck converter system effectively, ensuring favorable stability and robustness outcomes. Many of these methodologies have demonstrated commendable achievements in this endeavor. In this context, the suggested approach involving the OCSAPS algorithm for FOPID-controlled buck converter systems was evaluated alongside other algorithms listed in Table 8.

Table 8 comprehensively compares the proposed algorithm and other methods previously presented in the relevant domain. This evaluation encompasses diverse metrics associated with transient response, encompassing overshoot, rise time, settling time, and peak time, along with frequency response parameters like gain margin, phase margin, and bandwidth. The analysis underscores that, except in phase margin, the proposed algorithm outperforms these previously published approaches across both transient and frequency response criteria. As such, the data presented in Table 8 distinctly substantiates the proposed algorithm's superior performance compared to its counterparts.

***Table 8.*** *Comparison of transient and frequency response measures of some of the most effective algorithms for FOPID controllers documented in the literature.*

| Controller type | Maximum overshoot (%) | Rise time (s) | Settling time (s) | Peak time (s) | Gain margin (dB) | Phase margin (deg) | Bandwidth (Hz) |
|---|---|---|---|---|---|---|---|
| **OCSAPS-FOPID** | **0** | **$2.6081x10^{-7}$** | **$4.6467x10^{-7}$** | **$6.8863x10^{-7}$** | **Inf.** | 89.9970 | **$8.4051x10^{6}$** |
| CSA-FOPID | **0** | $3.2880x10^{-7}$ | $5.8550x10^{-7}$ | $8.6839x10^{-7}$ | **inf.** | 89.9882 | $6.6660x10^{6}$ |
| IHGS-FOPID (Izci & Ekinci, 2022) | **0** | $2.8510x10^{-7}$ | $5.0765x10^{-7}$ | $1.3686x10^{-6}$ | **Inf.** | 89.9995 | $7,6879x10^{6}$ |
| LFDSA-FOPID (Izci et al., 2022a) | **0** | $3.5068x10^{-7}$ | $6.2519x10^{-7}$ | $1.6823x10^{-6}$ | **Inf.** | **90.0081** | $6.2520x10^{6}$ |
| LFD-FOPID (Izci et al., 2022a) | **0** | $4.0260x10^{-7}$ | $7.1709x10^{-7}$ | $1.9322x10^{-6}$ | **Inf.** | 90.0020 | $5.4445x10^{6}$ |
| ABC-FOPID (Izci et al., 2022a)) | **0** | $4.2808x10^{-7}$ | $7.6297x10^{-7}$ | $2.0539x10^{-6}$ | **Inf.** | 90.0063 | $5.1212x10^{6}$ |
| PSO-FOPID (Izci et al., 2022a) | **0** | $4.6066x10^{-7}$ | $8.2062x10^{-7}$ | $2.2108x10^{-6}$ | **Inf.** | 90.0029 | $4.7584x10^{6}$ |

## 7. CONCLUSION

A new method, the OCSAPS algorithm, presents a novel hybrid metaheuristic approach for enhancing the efficiency of controlling a FOPID controller in a buck converter system. This novel approach integrates the OBL mechanism and the PS algorithm, enhancing the exploration and exploitation abilities of the original CSA. Statistical boxplot and convergence response analyses were conducted to establish the superiority of OCSAPS over CSA. Furthermore, the effectiveness of the proposed algorithm-based FOPID controller in the buck converter system was compared to established algorithms like HHO, GA, and CSA, using comprehensive testing such as transient and frequency response analysis and robustness assessment. Across these evaluations, the OCSAPS algorithm-based FOPID-controlled buck converter system demonstrated remarkable robustness, stability, and efficiency, outperforming its counterparts. Moreover, the proposed approach was compared with six other approaches regarding time and frequency domain responses. This comparative analysis affirmed the OCSAPS approach's exceptional performance, solidifying its preeminence in the relevant field. This innovative algorithm can also optimize various controllers in different systems, such as DC motor speed control, battery voltage management systems, and cruise control systems, which could be subject to investigation in future studies.

## CONFLICT OF INTEREST

The authors declare no conflict of interest.

## REFERENCES

Al-Majidi, S. D., Abbod, M. F., & Al-Raweshidy H. S. (2019). Design of an Efficient Maximum Power Point Tracker Based on ANFIS Using an Experimental Photovoltaic System Data. *Electronics*, *8*(8), 858. https://www.doi.org/10.3390/electronics8080858

Boudjehem, B., & Boudjehem, D. (2016). Fractional PID Controller Design Based on Minimizing Performance indices. *IFAC-PapersOnLine*, *49*(9), 164-168. https://www.doi.org/10.1016/j.ifacol.2016.07.522

Cech, M., & Schlegel, M. (2013, February 25-28). *Generalized robust stability regions for fractional PID controllers*. In: Proceedings of the 2013 IEEE International Conference on Industrial Technology (ICIT), (pp. 76-81). https://www.doi.org/10.1109/ICIT.2013.6505651

Chevalier, A., Francis, C., Copot, C., Ionescu, C. M., & Keyser, R. D. (2019). Fractional-order PID design: Towards transition from state-of-art to state-of-use. *ISA Transactions*, *84*, 178-186. https://www.doi.org/10.1016/j.isatra.2018.09.017

Das, S., Pan, I., Das, S., & Gupta, A. (2012). A novel fractional order fuzzy PID controller and its optimal time domain tuning based on integral performance indices. *Engineering Applications of Artificial Intelligence*, *25*(2), 430-442. https://www.doi.org/10.1016/j.engappai.2011.10.004

Dastjerdi, A. A., Vinagre, B. M., Chen, Y. Q., & HosseinNia, S. H. (2019). Linear fractional order controllers; A survey in the frequency domain. *Annual Reviews in Control*, *47*, 51-70. https://www.doi.org/10.1016/j.arcontrol.2019.03.008

Demir, M. H., & Demirok, M. (2023). Designs of Particle-Swarm-Optimization-Based Intelligent PID Controllers and DC/DC Buck Converters for PEM Fuel-Cell-Powered Four-Wheeled Automated Guided Vehicle. *Applied Sciences*, *13*(5), 2919. https://www.doi.org/10.3390/app13052919

Dolai, S. K., Mondal, A., & Sarkar, P. (2022). Discretization of Fractional Order Operator in Delta Domain. *Gazi University Journal of Science Part A: Engineering and Innovation*, *9*(4), 401-420. https://www.doi.org/10.54287/gujsa.1167156

Erickson, R. W., & Maksimović, D. (2000). *Fundamentals of Power Electronics* (Second Edition). Springer.

Eshaghi, S., & Tavazoei, M. S. (2023). Finiteness conditions for performance indices in generalized fractional-order systems defined based on the regularized Prabhakar derivative. *Communications in Nonlinear Science and Numerical Simulation*, *117*, 106979. https://www.doi.org/10.1016/j.cnsns.2022.106979

Feng, Z., Niu, W., & Liu, S. (2021). Cooperation Search Algorithm: A Novel Metaheuristic Evolutionary Intelligence Algorithm for Numerical Optimization and Engineering Optimization Problems. *Applied Soft Computing*, *98*, 106734. https://www.doi.org/10.1016/j.asoc.2020.106734

Feng, Z. K., Shi, P. F., Yang, T., Niu, W. J., Zhou, J. Z., & Cheng, C. T. (2022). Parallel cooperation search algorithm and artificial intelligence method for streamflow time series forecasting. *Journal of Hydrology*, *606*, 127434. https://www.doi.org/10.1016/j.jhydrol.2022.127434

Gaing, Z. L. (2004). A Particle Swarm Optimization Approach for Optimum Design of PID Controller in AVR System. *IEEE Transactions on Energy Conversion*, *19*(2), 384-391. https://www.doi.org/10.1109/TEC.2003.821821

Hekimoğlu, B. (2019). Optimal Tuning of Fractional Order PID Controller for DC Motor Speed Control via Chaotic Atom Search Optimization Algorithm. *IEEE Access*, *7*, 38100-38114. https://www.doi.org/10.1109/ACCESS.2019.2905961

Hekimoğlu, B. (2023). Determination of AVR System PID Controller Parameters Using Improved Variants of Reptile Search Algorithm and a Novel Objective Function. *Energy Engineering*, *120*(7), 1515-1540. https://www.doi.org/10.32604/ee.2023.029024

Hekimoğlu, B., & Ekinci, S. (2020). Optimally Designed PID Controller for A DC-DC Buck Converter via A Hybrid Whale Optimization Algorithm with Simulated Annealing. *Electrica*, *20*(1), 19-27. https://www.doi.org/10.5152/electrica.2020.19034

Hsieh, C. H., & Chou, J. H. (2007). Design of optimal PID controllers for pwm feedback systems with bilinear plants. *IEEE Transactions on Control Systems Technology*, *15*(6), 1075-1079. https://www.doi.org/10.1109/TCST.2007.908084

Izci, D., & Ekinci, S. (2022). A novel improved version of hunger games search algorithm for function optimization and efficient controller design of buck converter system. *e-Prime - Advances in Electrical Engineering, Electronics and Energy*, *2*, 100039. https://www.doi.org/10.1016/j.prime.2022.100039

Izci, D., Ekinci, S., & Hekimoğlu, B. (2022a). Fractional-Order PID Controller Design for Buck Converter System via Hybrid Lévy Flight Distribution and Simulated Annealing Algorithm. A*rabian Journal for Science and Engineering*, *47*, 13729-13747. https://www.doi.org/10.1007/s13369-021-06383-z

Izci, D., Ekinci, S., & Hekimoğlu, B. (2022b). A Novel Modified Lévy Flight Distribution Algorithm to Tune Proportional, Integral, Derivative and Acceleration Controller on Buck Converter System. *Transactions of the Institute of Measurement and Control*, *44*(2), 393-409. https://www.doi.org/10.1177/01423312211036591

Izci, D., Hekimoğlu, B., & Ekinci, S. (2022c). A New Artificial Ecosystem-Based Optimization Integrated with Nelder-Mead Method for PID Controller Design of Buck Converter. *Alexandria Engineering Journal*, *61*(3), 2030-2044. https://www.doi.org/10.1016/j.aej.2021.07.037

Izci, D., Ekinci, S., & Zeynelgil, H. L. (2023). Controlling an automatic voltage regulator using a novel Harris hawks and simulated annealing optimization technique. *Advanced Control for Applications: Engineering and Industrial Systems*, e121. https://www.doi.org/10.1002/adc2.121

Lee, Y. S., Wang, J. S., & Hui, S. Y. R. (1997). Modeling, Analysis, and Application of Buck Converters in Discontinuous-Input-Voltage Mode Operation. *IEEE Transactions on Power Electronics*, *12*(2), 350-360. https://www.doi.org/10.1109/63.558762

Li, Y., & Zhao, Y. (2015, May 23-25). *Memory identification of fractional order systems: Background and theory*. In: Proceedings of the 27th Chinese Control and Decision Conference (2015 CCDC), (pp. 1038-1043). https://www.doi.org/10.1109/CCDC.2015.7162070

Maâmar, B., & Rachid, M. (2014). IMC-PID-fractional-order-filter controllers design for integer order systems. *ISA Transactions*, *53*(5), 1620-1628. https://www.doi.org/10.1016/j.isatra.2014.05.007

Martinez-Patiño, L. M., Perez-Pinal, F. J., Soriano-Sánchez, A. G., Rico-Secades, M., Zarate-Orduño, C., & Nuñez-Perez, J. C. (2023). Fractional PID Controller for Voltage-Lift Converters. *Fractal and Fractional*, *7*(7), 542. https://www.doi.org/10.3390/fractalfract7070542

Micev, M., Ćalasan, M., & Oliva, D. (2020). Fractional Order PID Controller Design for an AVR System Using Chaotic Yellow Saddle Goatfish Algorithm. *Mathematics*, *8*(7), 1182. https://www.doi.org/10.3390/math8071182

Mohd Tumari, M. Z., Ahmad, M. A., Suid, M. H., & Hao, M. R. (2023). An Improved Marine Predators Algorithm-Tuned Fractional-Order PID Controller for Automatic Voltage Regulator System. *Fractal and Fractional*, *7*(7), 561. https://www.doi.org/10.3390/fractalfract7070561

Monje, C. A., Vinagre, B. M., Feliu, V., & Chen, Y. Q. (2008). Tuning and auto-tuning of fractional order controllers for industry applications. *Control Engineering Practice*, *16*, 798-812. https://www.doi.org/10.1016/j.conengprac.2007.08.006

Ortatepe, Z. (2023). Genetic Algorithm based PID Tuning Software Design and Implementation for a DC Motor Control System. *Gazi University Journal of Science Part A: Engineering and Innovation*, *10*(3), 286-300. https://www.doi.org/10.54287/gujsa.1342905

Ortiz-Quisbert, M. E., Duarte-Mermoud, M. A., Milla, F., Castro-Linares, R., & Lefranc, G. (2018). Optimal fractional order adaptive controllers for AVR applications. *Electrical Engineering*, *100*, 267-283. https://www.doi.org/10.1007/s00202-016-0502-2

Oustaloup, A., Levron, F., Mathieu B., & Nanot, F. M. (2000). Frequency-Band Complex Noninteger Differentiator: Characterization and Synthesis. *IEEE Transactions on Circuits and Systems I: Fundamental Theory and Applications*, *47*(1), 25-39. https://www.doi.org/10.1109/81.817385

Pan, F., & Liu, L. (2016, May 28-30). *Research on different integral performance indices applied on fractional-order systems*. In: Proceedings of the 2016 Chinese Control and Decision Conference (CCDC), (pp. 324-328). https://www.doi.org/10.1109/CCDC.2016.7531003

Podlubny, I. (1999). Fractional-Order Systems and PIλDμ-Controllers. *IEEE Transactions on Automatic Control*, *44*(1), 208-214. https://www.doi.org/10.1109/9.739144

Ranjan, A., & Mehta, U. (2023). Fractional-Order Tilt Integral Derivative Controller Design Using IMC Scheme for Unstable Time-Delay Processes. *Journal of Control, Automation and Electrical Systems*, *34*, 907-925. https://www.doi.org/10.1007/s40313-023-01020-6

Sangeetha, S., Sri Revathi, B., Balamurugan, K., & Suresh G. (2023). Performance analysis of buck converter with fractional PID controller using hybrid technique. *Robotics and Autonomous Systems*, *169*, 104515. https://www.doi.org/10.1016/j.robot.2023.104515

Shah, P., & Agashe, S. (2016). Review of fractional PID controller. *Mechatronics*, *38*, 29-41. https://www.doi.org/10.1016/j.mechatronics.2016.06.005

Smedley, K., & Cuk, S. (1994). Switching Flow-Graph Nonlinear Modeling Technique. *IEEE Transactions on Power Electronics*, *9*(4), 405-413. https://www.doi.org/10.1109/63.318899

Tizhoosh, H. R. (2005, November 28-30). *Opposition-Based Learning: A New Scheme for Machine Intelligence*. In: Proceedings of the International Conference on Computational Intelligence for Modelling, Control and Automation and International Conference on Intelligent Agents, Web Technologies and Internet Commerce (CIMCA-IAWTIC'06), (pp. 695-701). https://www.doi.org/10.1109/CIMCA.2005.1631345

Torczon, V. (1989). *Multi-Directional Search: A Direct Search Algorithm for Parallel Machines*. PhD Thesis, Rice University, Houston, Texas, USA.

Torczon, V. (1997). On the Convergence of Pattern Search Algorithms. *SIAM Journal on Optimization*, *7*(1), 1-25. https://www.doi.org/10.1137/S1052623493250780

Wang, Z., Li, S., Wang, J., & Li, Q. (2017). Robust control for disturbed buck converters based on two GPI observers. *Control Engineering Practice*, *66*, 13-22. https://www.doi.org/10.1016/j.conengprac.2017.06.001

Warrier, P., & Shah, P. (2021). Optimal Fractional PID Controller for Buck Converter Using Cohort Intelligent Algorithm. *Applied System Innovation*, *4*(3):50. https://www.doi.org/10.3390/asi4030050

Zhang, B., & Qiu, D. (2014). Sneak Circuits of DC-DC Converters. In: *Sneak Circuits of Power Electronic Converters* (pp. 59-103). IEEE. https://www.doi.org/10.1002/9781118379950.ch3